Dalton Transactions

Computational analysis of metal-metal bonded dimetal tetrabenzoate redox potentials in the context of ammonia oxidation electrocatalysis

Journal:	*Dalton Transactions*
Manuscript ID	DT-ART-02-2023-000552.R1
Article Type:	Paper
Date Submitted by the Author:	17-Apr-2023
Complete List of Authors:	Pavelic, Alex; University of Wisconsin, Chemistry Trenerry, Michael; University of Wisconsin, Chemistry Berry, John; University of Wisconsin, Chemistry

ARTICLE

Computational analysis of metal-metal bonded dimetal tetrabenzoate redox potentials in the context of ammonia oxidation electrocatalysis

Received 00th January 20xx,
Accepted 00th January 20xx

DOI: 10.1039/x0xx00000x

Alex M. Pavelic,[a] Michael J. Trenerry [a] and John F. Berry*[a]

Metal-metal bonded complexes are promising candidates for catalyzing redox transformations. Of particular interest is the oxidation of ammonia to dinitrogen, an important half reaction for the potential utilization of ammonia as a fuel or hydrogen carrier. This work computationally explores 30 different metal-metal bonded dimers (5 different metal centers and 6 different benzoate ligand derivatives) to explore the tunability of the redox potential when ammonia is bound to the complexes as an axial ligand, modeling the first step in ammonia oxidation electrocatalysis. We calculate the redox potentials of these compounds, making reference to experimental data when appropriate, identifying two degrees of tunability: a coarse adjustment, changing the metal center, allows for a wide range of redox potentials to be accessed (from +1.0 to –2.0 V vs ferrocene/ferrocenium in acetonitrile solution) and a fine adjustment, the para-substituent of the benzoate derivative, which affects the redox potential in a smaller range based on the electron donating/withdrawing effects of the substituent. Ruthenium and osmium tetrabenzoate catalysts are prime candidates for next generation ammonia oxidation catalysts because their redox potentials fall within the direct ammonia fuel cell "viability zone" bracketed by the thermodynamic potentials of oxygen reduction (ORR) and nitrogen reduction (NRR). Rhodium tetrabenzoate species fall above the ORR potential, suggesting ammonia oxidation promoted by Rh_2 catalysts could instead be used to facillitate hydrogen production through coupling to hydrogen evolution at a cathode. The redox potentials of rhenium and iridium tetrabenzoate catalysts fall below the NRR potential suggesting that these compounds could be further investigated in the context of electrochemical ammonia synthesis. Each redox event studied involves electron transfer from the M–M δ* orbital regardless of choice of metal or benzoate ligand derivative; this leads us to believe that the chemical reactivity of the various studied compounds will be similar in the context of ammonia oxidation.

Introduction

Development of alternative fuels from renewable sources is required to achieve carbon-neutrality,[1–3] and the "Nitrogen Economy" has emerged as a potential solution to this existential problem,[4,5] motivating fundamental research in electrochemical ammonia synthesis and the utilization of ammonia as an energy source, ideally in direct ammonia fuel cells (DAFCs). There are currently a small, but rapidly growing number of molecular catalysts capable of performing the ammonia oxidation reaction (AOR),[6–15] and the search for more viable catalysts is an important fundamental research goal. By coupling electrocatalytic AOR to a cathode process, ammonia may either be used as a "hydrogen carrier" or directly as a chemical fuel. The viability of these processes, outlined in Chart 1, depends on the applied potentials at which a catalyst promotes ammonia oxidation. Many AOR catalysts promote reactivity only at larger overpotentials, and thus require applied potentials higher than the thermodynamic potential for the oxygen reduction reaction (ORR). Catalysts that operate in this thermodynamic regime have been used for the in-situ electrochemical decomposition of ammonia into nitrogen and hydrogen at a mild applied potential (top of Chart 1), [14] effectively using ammonia as a hydrogen carrier rather than a primary fuel. We recently discovered a metal-metal bonded Ru_2 complex, $Ru_2(chp)_4(NH_3)^+$ (**1**, chp = 2-chloro-6-hydroxypyridinate), that promotes electrocatalytic ammonia oxidation at sufficiently low

Ammonia as a Hydrogen Carrier:

Anode: $N_2\,(g) + 6\,H^+\,(aq) + 6\,e^- \longrightarrow 2\,NH_3\,(aq)$ $E^o_{an} = +0.092$ V

Cathode: $2\,H^+\,(aq) + 2\,e^- \longrightarrow H_2\,(g)$ $E^o_{cat} = 0.000$ V

$E^o_{Cell} = E^o_{cat} - E^o_{an} = -0.092$ V

Ammonia as a Fuel:

Anode: $N_2\,(g) + 6\,H^+\,(aq) + 6\,e^- \longrightarrow 2\,NH_3\,(aq)$ $E^o_{an} = +0.092$ V

Cathode: $O_2\,(g) + 4\,H^+\,(aq) + 4\,e^- \longrightarrow 2\,H_2O\,(l)$ $E^o_{cat} = +1.229$ V

$E^o_{Cell} = E^o_{cat} - E^o_{an} = +1.137$ V

Chart 1. Thermodynamic analysis of electrochemical ammonia utilization with potentials in V vs NHE. Half reactions are written as reductions by convention with the associated thermodynamic potentials.

[a] *Department of Chemistry, University of Wisconsin-Madison, 1101 University Avenue, Madison, Wisconsin 53706, USA Address here.*
Electronic Supplementary Information (ESI) available: Calculated structures, redox potentials, and representative orbitals. See DOI: 10.1039/x0xx00000x

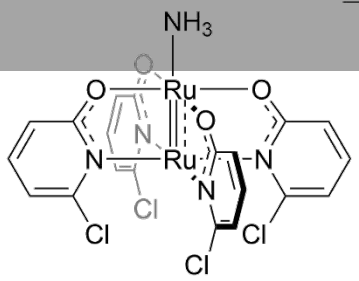

(**1**)

This Work

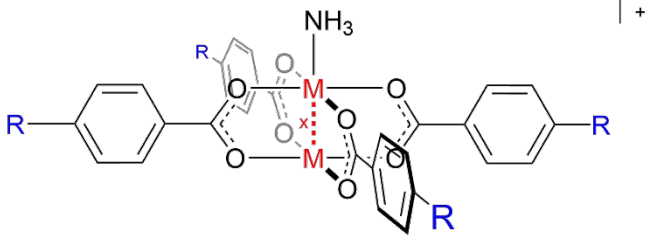

M = Ru (**2**), Os (**3**), Rh (**4**), Ir (**5**), Re* (**6**)
R = Br (**a**), Cl (**b**), F (**c**), H (**d**), Me (**e**), NMe_2 (**f**)

x Bond Order: 2.5 = Ru, Os; 1.5 = Rh, Ir; 3.5 = Re

overpotentials, such that this process can be coupled with oxygen reduction to give a net exergonic reaction, as is needed for a productive fuel cell (bottom of Chart 1).[9] We are currently working to understand the mechanism of ammonia oxidation by **1**,[16] and to identify new bimetallic catalysts that improve on both thermodynamic and kinetic issues.

Fig. 1. **1** and the survey of bimetallic tetrabenzoate paddlewheel complexes considered in this work with varying metal center and para-substitution of the equatorial benzoate ligand. Para substituents, R, are listed in order of most positive to most negative Hammett parameter. *$Re_2^{5+/6+}$ is analyzed in this study, instead of $Re_2^{4+/5+}$.

Our previous study of **1** indicated that electrocatalytic ammonia oxidation operates at the $Ru_2^{4+/5+}$ redox potential, where facile one-electron oxidation of Ru_2^{4+} at the working electrode is followed by a spontaneous redox reaction between Ru_2^{5+} and exogenous ammonia, yielding dinitrogen and ammonium products while regenerating the reduced Ru_2^{4+} electrocatalyst species. This work also included a preliminary computational analysis highlighting the importance of metal-metal antibonding orbitals in facilitating both processes. The reduced Ru_2^{4+} and oxidized Ru_2^{5+} electrocatalyst species respectively possess full and half-filled Ru–Ru δ^*orbitals, the energies of which dictate the operating potential of electrocatalysis. Delocalization of a π^* orbital across the Ru–Ru–N axis of a crucial Ru–Ru–NH_2 intermediate was proposed to enable N–N bond formation via nucleophilic attack of ammonia.[9] However, the impact of substituting ruthenium with other second and third row transition metals within this bimetallic design has yet to be determined, and insights into how equatorial ligand electronics influence the redox behaviour of these bimetallic cores is also desirable. By increasing the breadth of our computational study to include different combinations of bimetallic core and equatorial ligand identities, we connect periodic trends with the predicted overpotentials of candidate second-generation electrocatalysts and thus establish design principles for ammonia oxidation electrocatalysts based on this unique bimetallic paddlewheel motif.

In this work, we describe a broad computational investigation examining the predicted redox potentials of bimetallic tetrabenzoate paddlewheel complexes $[M_2(Bz)_4(NH_3)]^+$, where Bz = a para-substituted benzoate. These compounds are respectively labelled as **2 – 6** for M = Ru, Os, Rh, Re, Ir, with letters **a – f** denoting the para substituents of Bz: Br, Cl, F, H, Me, NMe_2 (Fig. 1). These bimetallic cores are investigated due to their prevalence in previously reported systems[17] and their similarity to **1** in terms of general electronic structure. Notably, tetracarboxylate complexes are known for all of these bimetallic cores except Ir_2, though only Ru_2 and Rh_2 carboxylate complexes are reported in both the M_2^{4+} and M_2^{5+} oxidation states. Several of the species considered in this work are thus predicted compounds that expand upon a familiar structural motif. Homoleptic Ru_2 tetrabenzoate complexes have recently been explored in coordination polymers,[18–52] liquid crystals,[53] charge-transfer complexes,[54,55] as oxidation catalysts,[56–58] and the redox properties of several Ru_2 benzoate derivatives have been studied.[59–66] Rh_2 benzoate-derived complexes have been examined for their host-guest,[67–75] structural,[76–84] light absorbing,[85–87] catalytic,[88,89] kinetic,[90] and hydrogen evolution properties.[91] Dirhenium tetrabenzoate is known in the Re_2^{6+} oxidation state with two chloride axial ligands.[92] Similarly, Os_2^{6+} tetrabenzoate derivatives are known as bis-axial Cl complexes.[93,94]

The functionalization of benzoate equatorial ligands enables further tunability and finer control over the redox potentials of candidate electrocatalyst structures beyond leveraging bimetallic core identities. Focusing on para-substituted benzoates, we investigate a range of electron-withdrawing and electron-donating groups to better understand and quantify the influence of ligand electronics on these redox potentials. Additionally, the use of para-substituted benzoate ligands permits axial binding of ammonia at two potential active sites as opposed to only one in **1**, which we anticipate may improve the kinetics of electrocatalysis.

Methods

Geometry optimization and vibrational frequency calculations were performed by density functional theory using the ORCA computational platform (version 4.2.1) for 30 different bimetallic tetrabenzoate compounds with one axially bound ammonia ligand.[95] Compounds in the $[M_2]^{4+}$ and $[M_2]^{5+}$ oxidation states are considered for series **2**-**5**. For series **6**, compounds in the $[Re_2]^{5+}$ and $[Re_2]^{6+}$ oxidation states were examined instead due to convergence issues in the calculation of $[Re_2]^{4+}$ species. The most energetically favorable spin states were considered in each case: ruthenium and osmium complexes were studied in the high spin $S = 1$ configuration for $[M_2]^{4+}$ and in the high spin $S = 3/2$ spin state configuration for $[M_2]^{5+}$;[9] rhodium, iridium, and rhenium complexes were studied in the low spin state configuration regardless of oxidation state: $S = 0$ for Re_2^{6+}, Rh_2^{4+}, and Ir_2^{4+}; $S = 1/2$ for M_2^{5+} complexes. Initial geometries were originally obtained by altering coordinates from previous geometry data of **1** and were subsequently optimized to a very tight convergence criterion (ETol = 1.0×10^{-9} Ha). Calculations were performed using the BP86 functional, which has been shown to give as good accuracy as hybrid functionals for the calculation of redox potentials in **1** and other transition metal systems (see

Supplementary Information).[96–98] The ZORA-def2-SVP basis set combined with a SARC/J auxiliary basis set was used to model the complexes, and a larger SARC-ZORA-TZVP basis set was used for the metal atoms to more accurately model the unique electronic structure of the metal-metal bond, including relativistic effects.[99–102] The solvent environment was modeled with the conductor-like polarizable continuum model (CPCM) to account for solvation effects of acetonitrile.[103] Choice of functional, basis set, and modeling parameters were made after the results of preliminary tests on the performance of different DFT functionals with respect to the energetic properties, structural properties, and computing time for these molecular systems of up to 90 atoms.

$$E_{1/2} = -\frac{(G_{M_2^{4+}} + G_{Fc^+}) - (G_{M_2^{5+}} + G_{Fc})}{F \cdot n}$$

Equation 1. Equation describing the calculation of an $M_2^{4+/5+}$ redox potential, $E_{1/2}$, vs Fc/Fc^+ from the change in Gibbs free energy at 298 K (ΔG), using Faraday's constant (F) and number of electrons (n).

The redox potential of the $M_2^{4+/5+}$ couple (or $M_2^{5+/6+}$ for M = Re) was evaluated by calculating the Gibbs free energy (G) of each species with respect to the ferrocene/ferrocenium redox couple (Fc/Fc^+) using Equation 1,[104] then cathodically shifted by 346 mV to account for the difference between the resulting computed redox potential and the measured redox potential of model compound **1** (see Supplementary Information). Within each series of compounds, the predicted redox potentials were plotted against Hammett parameters of the substituted benzoate derivatives, which quantify the degree of ligand electron-donating or electron-withdrawing character arising from the substituent in the para position.[105]

M	M^{2+}–M^{2+} (Å)	M^{2+}–M^{3+} (Å)	M_2^{4+}–NH_3 (Å)	M_2^{5+}–NH_3 (Å)	M_2^{4+}–O (Å)	M_2^{5+}–O (Å)	M_2^{4+} θ_1 (°)	M_2^{5+} θ_1 (°)	M_2^{4+} θ_2 (°)	M_2^{5+} θ_2 (°)
Ru	2.292	2.286	2.244	2.209	2.067	2.024	0.037	0.029	0.032	0.018
Os	2.362	2.346	2.256	2.229	2.082	2.040	0.040	0.019	0.037	0.038
Rh	2.412	2.398	2.169	2.136	2.049	2.017	0.041	0.059	0.028	0.106
Ir	2.468	2.442	2.180	2.154	2.066	2.032	0.046	0.173	0.040	0.797
M	M^{2+}–M^{3+} (Å)	M^{3+}–M^{3+} (Å)	M_2^{5+}–NH_3 (Å)	M_2^{6+}–NH_3 (Å)	M_2^{5+}–O (Å)	M_2^{6+}–O (Å)	M_2^{5+} θ_1 (°)	M_2^{6+} θ_1 (°)	M_2^{5+} θ_2 (°)	M_2^{6+} θ_2 (°)
Re	2.208	2.209	2.326	2.291	2.057	2.010	0.034	0.042	0.018	0.041

Table 1. Key bond lengths and angles for the optimized benzoate (**d**) structures in series **2**-**6**. A complete table of all complexes analyzed can be found in the Supplementary Information. For the purpose of distinguishing between the metal atoms in the table below, "M^{2+}" refers to the metal atom that is not bonded to the NH_3 ligand and "M^{3+}" refers to the metal atom bonded to the NH_3 ligand. It should be noted though that these assignments of oxidation number are artificial, since the mixed-valent species are necessarily fully delocalized due to the metal-metal bond. O–M–M–O torsion angles (θ_1) were measured by averaging the four dihedral angles of the metal center coordinated to each carboxylate. Ligand torsion angles (θ_2) were measured by averaging the four dihedral angles between the phenyl ring plane and the carboxylate plane on each benzoate ligand (see Fig. 2). R groups are organized from largest positive para-effect to largest negative para-effect (**a**-**f**).

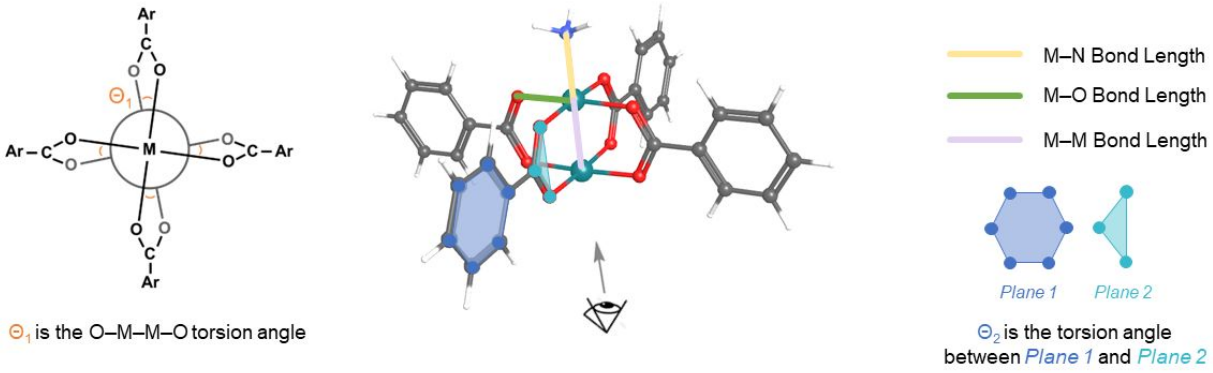

Fig 2. Illustration of key bond lengths and angles analyzed in Table 1.

Results

Geometry information for the mono-ammine complexes is shown in Table 1. M–M bond distances in **2**, **4**, and **6** align with previous crystallographic data of M_2^{4+} carboxylates.[106–108] For Re, only few Re_2^{6+} carboxylate complexes are known, which typically contain halide or other X-type axial ligands; nevertheless the Re–Re distances in the calculated Re_2^{6+} and Re_2^{5+} structures are only ~0.03 Å shorter than those of the known Re_2^{6+} compounds.[92,109,110] Os_2^{4+} and Os_2^{5+} carboxylate complexes are not known, though Os_2^{6+} carboxylates are. The calculated Os–Os distances for Os_2^{4+} and Os_2^{5+} species are consistently greater than those of reported Os_2^{6+} complexes, consistent with a lower Os–Os bond order of the reduced Os_2 core.[94] Comparison with experiment is difficult in the case of Ir since Ir_2 tetracarboxylate complexes are unknown. However, the fact that the Ir–Ir distances calculated here are the longest reported in our series agrees well with structural comparisons of metal-metal bonded complexes supported by formamidinate ligands.[111] Ir_2 tetraformamidinate complexes are known in both the Ir_2^{4+} and Ir_2^{5+} oxidation states,[111,112] and show an increase in Ir–Ir distance upon oxidation that is not reproduced here, but this discrepancy could be due to the fact that the known Ir_2^{4+} compounds do not contain axial ligands and the Ir_2^{5+} complexes do. Decrease in M–M bond lengths of **2–5** upon oxidation from M_2^{4+} to M_2^{5+} indicates that the electron being removed in each case originates from an M–M antibonding orbital; bond contraction occurs despite an increase in electrostatic repulsion between the more positively charged metal centers.[113] The lack of change in M–M bond lengths upon oxidation of **6** from Re_2^{5+} to Re_2^{6+} shows that in this case both the electrostatic effect and the change in metal-metal bond order equally balance.

The M–M and M–NH_3 bond lengths correlate with periodic trends in an interesting way, as highlighted in Figure 3. For any given metal, species in higher oxidation states display a shortened axial M–NH_3 bond, and equatorial M–O bond lengths are shortened to a similar degree. M–M bond distances lengthen and M–NH_3 bonds contract with the increased of period and group number of M. If only atomic size were considered, then only a contraction of distances around each metal with increasing group number would be expected. This effect of increasing effective nuclear charge is best seen in the trend in M–O distances to the equatorial ligands across compounds **2** – **6**. Comparing M_2^{5+} species, the average M–O equatorial bond distances contract from 2.05 Å for Re_2 species in series **6** to distances of 2.03 Å and 2.04 Å in Rh_2 (series **4**) and Ir_2 (series **5**) species, respectively. M–NH_3 axial bond distances display a similar trend but with more pronounced contraction due to the *trans* influence of the M–M multiple bond. Clearly, bonding to an axial NH_3 ligand requires the metals to share their σ-symmetry orbitals between M–M vs M–NH_3 bonding; the stronger the M–M multiple bond, the stronger the *trans* influence, and the longer the M–NH_3 bond. Notably, the M–M bond order changes from 3 to 2 to 1 for the M_2^{4+} complexes in groups 7, 8, and 9, respectively.

Fine-tuning of the equatorial ligands **a** – **f** yields minor geometric changes; increasing electron donating character in the equatorial carboxylates consistently decreases the M–M bond distances and increases the M–N bond distances. Across all examined metal and equatorial ligand identities, the torsion angle of the complexes around the metal-metal bonds θ_1 (Fig. 2) remains consistently small. The small torsion angles anticipate the presence of M–M δ orbital interactions between the metal centers of these compounds. Similarly, the small torsion angles within the benzoate ligands (θ_2 <1°, Fig. 2) allow good orbital overlap between benzoate π-systems and the M_2 δ-symmetry orbitals.

Predicted redox potentials of 30 different bimetallic paddlewheel complexes, each bearing an axially coordinated ammonia ligand, are plotted versus the sum of Hammett parameters σ_p for their respective para-substituted benzoate equatorial ligands in Figure 4. Data are grouped and analyzed according to metal identity, with linear regression statistics summarized in Table 2. We chose to analyze redox potentials of the mono-ammine adducts due to their similarity to **1** and for

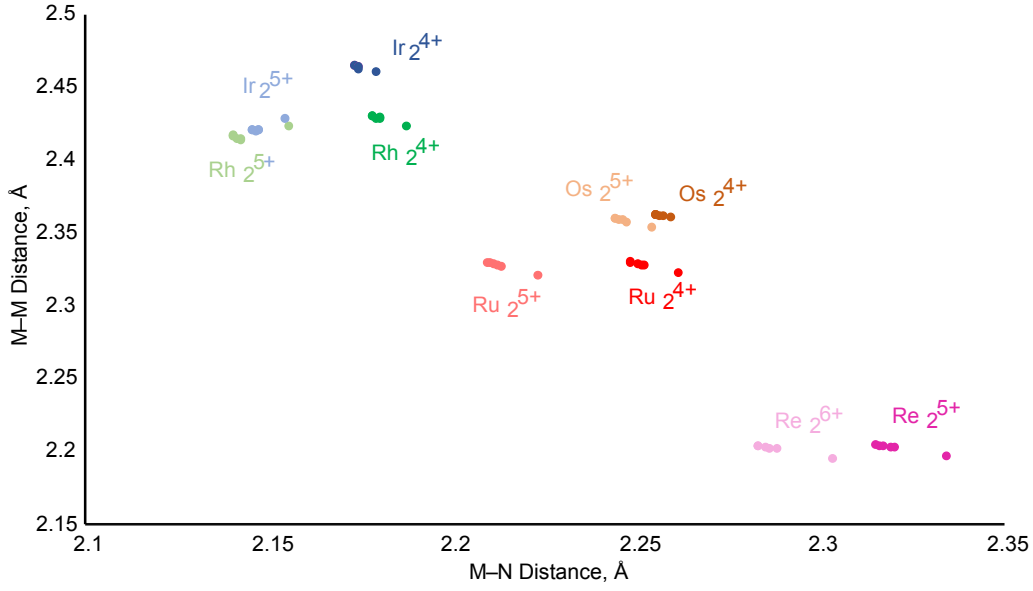

Fig. 3. Plot of the optimized M–M versus M–NH_3 distance for all of the compounds examined here.

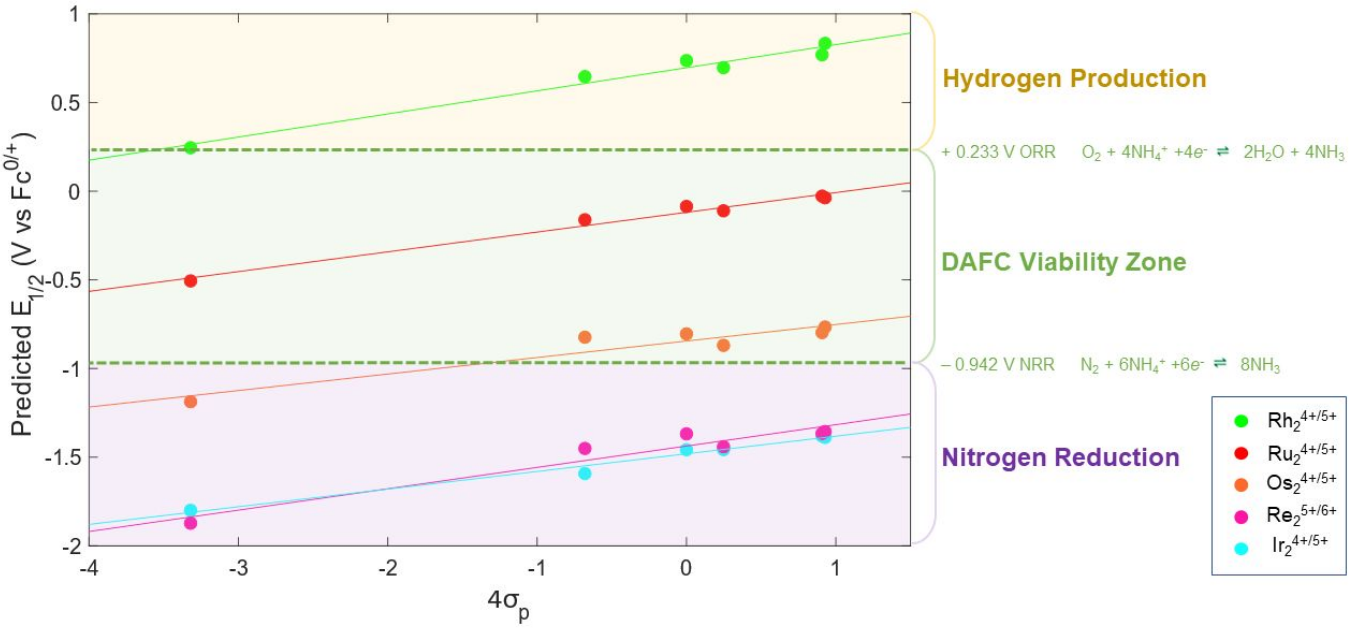

Fig. 4. Computationally-predicted redox potentials versus the sum of para-substituent Hammett parameters for benzoate equatorial ligands. Each point is shifted 346 mV cathodic to account for the offset between experimental and computational results (see SI). Data points and lines of best fit are coloured according to the identity of the bimetallic core in each complex. The light green region between potentials 0.233 V and -0.942 V vs $Fc^{0/+}$ represents the DAFC Viability Zone.

computational expedience; calculation of selected redox potentials of bis-ammine adducts indicated that their redox potentials are within ± 0.4 V of the mono-ammine adducts (see Supplementary Information). In Figure 4, we see that changing the metal center is predicted to drastically shift the redox potential of the complex, while benzoate substitution provides a means of fine-tuning the redox potentials of these complexes for a given metal center.

It is instructive to compare the slopes in Figure 4 to those of substituted $M_2(form)_4$ complexes (form = N,N'-diaryl-formamidinate) compiled by T. Ren,[114] and for the series of Ru_2[60,62,64,66] benzoate complexes that has been experimentally analyzed. Our computed Ru_2 redox potentials consistently predict a higher impact of *para* substitution with a larger slope than experimental studies (**2** ρ = 111.4 mV vs Miyasaka 2018 ρ = 81.3 mV and Miyasaka 2015 ρ = 91.5 mV).[64,66] This larger slope could be explained by our computations predicting both ligand (θ_2) and metal (θ_1) torsion angles for all complexes to be <1°, whereas crystallographic data of Ru_2 and Rh_2 tetrabenzoates show larger ligand torsion angles from 1-2° and metal torsion angles from 5-15°,[60,62,66,75,82] which hinder the aryl-π-to-metal-δ interaction. Computationally, slopes with optimal correlation coefficients in series **2**-**6** exhibit larger reaction constant (ρ) values than the tetraformamidinate series studied by Ren. Direct comparison of **2** and **4** to Ren's Ru_2 and Rh_2 tetraformamidinate series, respectfully, show that both carboxylate series have significantly greater redox potential tunability with a larger slope (**2** ρ = 111.4 mV, $Ru_2(form)_4Cl$ ρ = 70 mV; **4** ρ = 130.3 mV, $Rh_2(form)_4$ ρ = 98 mV).[114] The rigid twist angle and relative benzoate planarity in the geometry of these complexes allows for optimal overlap of benzoate π conjugation into the δ and δ* orbitals of the metal centers, which allows for variation in the functional group of the para-substituted site of the benzoate ligand to affect the redox event more than for other types of ligands. This effect is also apparent in complexes in series **3**, **5**, and **6**, as their ρ values range close to that of series **2** and **4**.

The choice of metal center is predicted to greatly affect the redox potentials of compounds investigated in this study. To assess the viability of these compounds as candidate electrocatalysts for

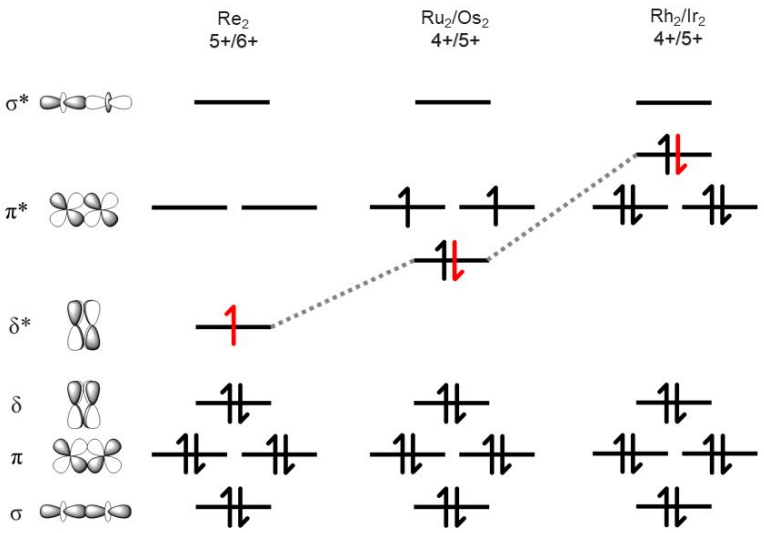

Fig. 5. Energy level visualization of redox couples within the metal-metal interactions of 5 different metal centers. Red half arrow represents the electron that is being removed during oxidation (M_2^{4+} to M_2^{5+} or M_2^{5+} to M_2^{6+}). Energy levels are not shown to scale.

ammonia oxidation, their predicted redox potentials are presented in the context of the thermodynamic standard potentials for ORR and NRR processes (DAFC viability zone in Figure 4), which bracket the range of potentials at which the electrocatalytic oxidation of ammonia must be facilitated in order to yield a productive fuel cell when coupled to oxygen reduction at a cathode. Thermodynamic ORR and NRR potentials are calculated for the conditions used in our previous work with **1**, using acetonitrile solvent with ammonium and ammonia acting as the conjugate acid/base pair involved in facilitating proton transfer. With the exception of **3f,** we observe that Ru_2 and Os_2 tetrabenzoates (series **2** and **3**, respectively) are the most promising AOR electrocatalyst candidates for fuel cell applications, as the $M_2^{4+/5+}$ redox couples for both sets of compounds lie within the DAFC viability zone. The $Rh_2^{4+/5+}$ potentials for series **4** are predicted to exceed the upper boundary of the DAFC viability zone as dictated by the thermodynamic ORR potential, but are in line with the operating potentials of other reported ammonia oxidation catalysts.[11,115] Rather than enabling a DAFC, electrocatalytic ammonia oxidation in this thermodynamic regime could instead be coupled to hydrogen evolution at a cathode and thus split ammonia into its constituent elements with mild applied potentials, as was first reported by Hamman, Smith, and coworkers.[14] Both the Re_2 and Ir_2 complexes as well as one Os complex (series **5**, **6**, and complex **3f**, respectively) possess redox potentials below the lower bound for DAFC viability as dictated by thermodynamic NRR potential, and could therefore be investigated as possible catalysts for electrochemical ammonia synthesis from nitrogen or hydrazine (the microscopic reverse of ammonia oxidation).

To better understand the trends in redox potentials for series **2 – 6**, we examine the electronic structures of the neutral and cationic species involved in each redox couple. Given the data in Figure 4, there are two key questions we seek to answer: First, what is the origin of the similar Hammett slope in series **2 – 6**? A second question arises upon examining the redox potentials of second-row and third-row transition metal analogues. Going from Ru_2 to Os_2 species, we predict a shift in redox potentials of approximately 0.7 V between analogous structures, consistent with trends reported for similar compounds.[116–118] However, the drop in potential between Rh_2 and Ir_2 species is approximately 2 V, posing the question of why Ir_2^{4+} compounds are predicted to be especially reducing relative to their Rh_2 congeners.

To address the first of these questions, we find from electronic structure analysis that, no matter the metal identity, each redox couple considered in this study involves an electron occupying an M–M δ* orbital, as shown in Figure 5. This result is consistent with previous electronic structure analysis of **1**, and is a reflection of the fact that the exact ordering of the metal-metal π* and δ* orbitals changes as the metal effective nuclear charge is increased. For Re, there is a significant splitting between the δ* and π* orbitals, as has been established for triply-bonded Re_2^{4+} compounds.[119,120] For Ru_2/Os_2, the δ* and π* orbitals are nearly degenerate, consistent with the "high spin" S = 3/2 ground states observed for Ru_2^{5+} and Os_2^{5+} compounds.[17] For Rh_2, EPR studies of simple Rh_2^{5+} carboxylates such as acetate have indicated an orbitally-degenerate π^{*3} ground state.[121,122] However, the Rh_2^{5+} complex supported by the more complicated esp bridging dicarboxylate ligand has been shown to have a δ^{*1} ground state due to interactions between the esp ligand orbitals and the Rh_2 δ* orbital.[123] We may attribute the δ^{*1} ground state in series **4** to the π-conjugation between the nearly-planar benzoate groups with the Rh_2 δ* orbital. The inversion of δ* and π* upon going from Re_2 to Ru_2/Os_2 to Rh_2/Ir_2 comes from the increase in effective nuclear charge of the metal centers that increases the energetic matching between later transition metals and ligand orbitals, in this case the δ* orbitals with the benzoate π system.

Addressing the second issue, studies by Ren and coworkers show that $Rh_2(form)_4$ derivatives possess redox potentials approximately 1 V higher than the analogous $Ru_2(form)_4$ complexes, consistent with our predictions for carboxylates considered in this study. However,

the lack of experimental data for Ir_2 complexes hinders our understanding of the large disparity in redox potentials between Ir_2 and Rh_2 complexes, and further study of this phenomenon and Ir_2 complexes in general is necessary. The unusually large difference in redox potentials predicted for Rh_2 versus Ir_2 compounds could underlie the lack of synthetic access to Ir_2 tetracarboxylates, as we note that at the time of this report, Ir^{3+} carboxylate compounds are exclusively known to adopt the oxo-centered trimetallic "basic" carboxylate structure.[124,125]

We also find that altering the electron-donating versus electron-withdrawing nature of equatorial benzoate ligands offers an additional degree of tunability over redox potentials. Consistently positive Hammett slopes across all metal identities show that more strongly electron-donating functional groups can be used to increase the electron density of the bimetallic core, and thus decrease the redox potential of the overall complex. Moreover, the magnitude of this effect is quite similar regardless of metal identity. This similarity arises from the universal involvement of an M–M δ* orbital in every redox event of the compounds considered in this study. When combined with the observation that M–M δ-symmetry orbitals overlap with the π-systems of equatorial benzoate ligands, the functionalization of these benzoate ligands provides a highly generalizable and systematic means of finely tuning redox potentials across this platform. Furthermore, the fact that each redox process involves the same M–M δ* orbital that is rigorously non-bonding with respect to the axial NH_3 ligand leads us to believe that the process of ammonia oxidation will be mechanistically similar across the different types of bimetallic cores described in this work. Collectively, these findings have profound implications for the future design of ammonia oxidation electrocatalysts.

This study of redox potentials was inspired from prior work in our research group on the Ru_2-based AOR electrocatalyst **1**, where the minimum applied potential required for promoting electrocatalytic ammonia oxidation from the reduced Ru_2^{4+} form of **1** closely matched the measured potential of its $Ru_2^{4+/5+}$ redox couple. However, we note that this initial one-electron oxidation may or may not be proton-coupled in other systems and thus impact the conditions required for achieving electrocatalysis. Future studies will thus address the possibility of proton-coupled electron transfer (PCET) events relevant to ammonia oxidation catalyzed by these systems and assess their impact on DAFC viability.

Conclusion

30 different bimetallic tetrabenzoate compounds, each bearing an axially coordinated ammonia ligand, were investigated by DFT as candidates for ammonia oxidation electrocatalysts. Based on predicted redox potentials, shown to be highly tunable according to metal and ligand identity, compounds were found to align with one of three thermodynamic regimes relevant to the future utilization of ammonia in an energy context. The redox potentials of Ru_2 and Os_2 complexes fall between the thermodynamic potentials for ORR and NRR processes, which bracket the operating potentials of ammonia oxidation catalysts viable for use in direct ammonia fuel cells. Rh_2 complexes possess redox potentials above the thermodynamic ORR potential, but may enable ammonia's use as a hydrogen carrier by electrochemical means via the coupling of electrocatalytic ammonia oxidation at an anode to hydrogen evolution at a cathode. Redox potentials of Re_2 and Ir_2 complexes are predicted to lie below the thermodynamic NRR potential, suggesting that these compounds could be further investigated in the context of electrochemical ammonia synthesis. The one-electron redox couples of all 30 complexes studied in this work involve an M–M δ* orbital, a finding that is consistent with the previously reported Ru_2 complex and known ammonia oxidation electrocatalyst **1**. Benzoate ligands with electron-donating substituents are predicted to provide fine control over these redox potentials in an array of bimetallic compounds and could enable electrocatalytic ammonia oxidation at reduced overpotentials, warranting further investigation. These findings illustrate the utility of computational methods in aiding the rational design of electrocatalysts for ammonia oxidation and motivate additional investigations of other reported AOR catalyst platforms.

Author Contributions

Alex Pavelic: performed calculations, wrote original draft. Michael Trenerry: guided research and supervision, review and editing. John Berry: guided research and project administration, review and editing.

Conflicts of interest

There are no conflicts to declare.

Acknowledgements

We thank the U.S. Department of Energy, Chemical Sciences, Geosciences, and Biosciences Division, Office of Basic Energy Sciences, Office of Science (DE-SC0021021). We also thank Trey Pankratz for assistance in performing calculations.

Notes and references

1 J. B. Zimmerman, P. T. Anastas, H. C. Erythropel and W. Leitner, *Science*, 2020, **367**, 397–400.

2 S. Sarp, S. Gonzalez Hernandez, C. Chen and S. W. Sheehan, *Joule*, 2021, **5**, 59–76.

3 A. J. Martín and J. Pérez-Ramírez, *Joule*, 2019, **3**, 2602–2621.

4 D. R. MacFarlane, P. V. Cherepanov, J. Choi, B. H. R. Suryanto, R. Y. Hodgetts, J. M. Bakker, F. M. Ferrero Vallana and A. N. Simonov, *Joule*, 2020, **4**, 1186–1205.

5 J. G. Chen, R. M. Crooks, L. C. Seefeldt, K. L. Bren, R. M. Bullock, M. Y. Darensbourg, P. L. Holland, B. Hoffman, M. J. Janik, A. K. Jones, M. G. Kanatzidis, P.

King, K. M. Lancaster, S. V. Lymar, P. Pfromm, W. F. Schneider and R. R. Schrock, *Science*, 2018, **360**, eaar6611.

6 P. L. Dunn, B. J. Cook, S. I. Johnson, A. M. Appel and R. M. Bullock, *J. Am. Chem. Soc.*, 2020, **142**, 17845–17858.

7 H.-Y. Liu, H. M. C. Lant, J. L. Troiano, G. Hu, B. Q. Mercado, R. H. Crabtree and G. W. Brudvig, *J. Am. Chem. Soc.*, 2022, **144**, 8449–8453.

8 Y. Li, J.-Y. Chen, Q. Miao, X. Yu, L. Feng, R.-Z. Liao, S. Ye, C.-H. Tung and W. Wang, *J. Am. Chem. Soc.*, 2022, **144**, 4365–4375.

9 M. J. Trenerry, C. M. Wallen, T. R. Brown, S. V. Park and J. F. Berry, *Nat. Chem.*, 2021, **13**, 1221–1227.

10 H. Toda, K. Kuroki, R. Kanega, S. Kuriyama, K. Nakajima, Y. Himeda, K. Sakata and Y. Nishibayashi, *ChemPlusChem*, 2021, **86**, 1511–1516.

11 M. D. Zott and J. C. Peters, *J. Am. Chem. Soc.*, 2021, **143**, 7612–7616.

12 P. Bhattacharya, Z. M. Heiden, G. M. Chambers, S. I. Johnson, R. M. Bullock and M. T. Mock, *Angew. Chem. Int. Ed.*, 2019, **58**, 11618–11624.

13 K. Nakajima, H. Toda, K. Sakata and Y. Nishibayashi, *Nat. Chem.*, 2019, **11**, 702–709.

14 F. Habibzadeh, S. L. Miller, T. W. Hamann and M. R. Smith, *Proc. Natl. Acad. Sci. U.S.A.*, 2019, **116**, 2849–2853.

15 M. E. Ahmed, M. Raghibi Boroujeni, P. Ghosh, C. Greene, S. Kundu, J. A. Bertke and T. H. Warren, *J. Am. Chem. Soc.*, 2022, **144**, 21136–21145.

16 M. J. Trenerry, C. M. Wallen, A. M. Wheaton and J. F. Berry, .

17 F. A. Cotton, C. A. Murillo, R. A. Walton and Eds., *Multiple Bonds between Metal Atoms*, Springer Science and Business Media, Inc., New York, 2005.

18 W.-Y. Gao, G. P. Van Trieste III and D. C. Powers, *Dalton Trans.*, 2020, **49**, 16077–16081.

19 C. Dou, W. Kosaka and H. Miyasaka, *Chem. Lett.*, 2017, **46**, 1288–1291.

20 W. Kosaka, Z. Liu and H. Miyasaka, *Dalton Trans.*, 2018, **47**, 11760–11768.

21 H. Miyasaka, T. Morita and M. Yamashita, *Chem. Commun.*, 2011, **47**, 271–273.

22 Y. Sekine, M. Nishio, T. Shimada, W. Kosaka and H. Miyasaka, *Inorg. Chem.*, 2021, **60**, 3046–3056.

23 W. R. Heinz, D. Staude, D. Mayer, H. Bunzen and R. A. Fischer, *Dalton Trans.*, 2021, **50**, 5226–5235.

24 H. Fukunaga, T. Yoshino, H. Sagayama, J. Yamaura, T. Arima, W. Kosaka and H. Miyasaka, *Chem. Commun.*, 2015, **51**, 7795–7798.

25 N. Motokawa, H. Miyasaka, M. Yamashita and K. R. Dunbar, *Angew. Chem. Int. Ed.*, 2008, **47**, 7760–7763.

26 H. Miyasaka, N. Motokawa, T. Chiyo, M. Takemura, M. Yamashita, H. Sagayama and T. Arima, *J. Am. Chem. Soc.*, 2011, **133**, 5338–5345.

27 M. Nishio and H. Miyasaka, *Inorg. Chem.*, 2014, **53**, 4716–4723.

28 W. Kosaka, T. Morita, T. Yokoyama, J. Zhang and H. Miyasaka, *Inorg. Chem.*, 2015, **54**, 1518–1527.

29 M. J. Murphy, T. D. Keene, J. R. Price, D. M. D'Alessandro and C. J. Kepert, *Aust. J. Chem.*, 2014, **67**, 1607.

30 K. Taniguchi, K. Narushima, K. Yamagishi, N. Shito, W. Kosaka and H. Miyasaka, *Jpn. J. Appl. Phys.*, 2017, **56**, 060307.

31 J. Zhang, W. Kosaka, Y. Kitagawa and H. Miyasaka, *Nat. Chem.*, 2021, **13**, 191–199.

32 K. Nakabayashi and H. Miyasaka, *Chem. Eur. J.*, 2014, **20**, 5121–5131.

33 J. Zhang, W. Kosaka, K. Sugimoto and H. Miyasaka, *J. Am. Chem. Soc.*, 2018, **140**, 5644–5652.

34 K. Taniguchi, K. Narushima, J. Mahin, W. Kosaka and H. Miyasaka, *Angew. Chem. Int. Ed.*, 2016, **55**, 5238–5242.

35 J. Zhang, W. Kosaka, H. Sato and H. Miyasaka, *J. Am. Chem. Soc.*, 2021, **143**, 7021–7031.

36 M. Abe, Y. Sasaki, T. Yamaguchi and T. Ito, *BCSJ*, 1992, **65**, 1585–1590.

37 K. Nakabayashi, M. Nishio and H. Miyasaka, *Inorg. Chem.*, 2016, **55**, 2473–2480.

38 W. Kosaka, M. Itoh and H. Miyasaka, *Mater. Chem. Front.*, 2018, **2**, 497–504.

39 N. Motokawa, T. Oyama, S. Matsunaga, H. Miyasaka, M. Yamashita and K. R. Dunbar, *CrystEngComm*, 2009, **11**, 2121.

40 M. C. Barral, R. González-Prieto, R. Jiménez-Aparicio, J. L. Priego, M. R. Torres and F. A. Urbanos, *Eur. J. Inorg. Chem.*, 2004, **2004**, 4491–4501.

41 G. Arribas, M. C. Barral, R. González-Prieto, R. Jiménez-Aparicio, J. L. Priego, M. R. Torres and F. A. Urbanos, *Inorg. Chem.*, 2005, **44**, 5770–5777.

42 Y. Sekine, T. Shimada and H. Miyasaka, *Chem. Eur. J.*, 2018, **24**, 13093–13097.

43 J. Zhang, W. Kosaka, Y. Kitagawa and H. Miyasaka, *Angew. Chem. Int. Ed.*, 2019, **58**, 7351–7356.

44 N. Motokawa, S. Matsunaga, S. Takaishi, H. Miyasaka, M. Yamashita and K. R. Dunbar, *J. Am. Chem. Soc.*, 2010, **132**, 11943–11951.

45 H. Fukunaga, W. Kosaka, H. Nemoto, K. Taniguchi, S. Kawaguchi, K. Sugimoto and H. Miyasaka, *Chem. Eur. J.*, 2020, **26**, 16755–16766.

46 J. Zhang, W. Kosaka, S. Kitagawa, M. Takata and H. Miyasaka, *Chem. Eur. J.*, 2019, **25**, 3020–3031.

47 J. Zhang, W. Kosaka, H. Fukunaga, S. Kitagawa, M. Takata and H. Miyasaka, *Inorg. Chem.*, 2016, **55**, 12085–12092.

48 W. Kosaka, Y. Takahashi, M. Nishio, K. Narushima, H. Fukunaga and H. Miyasaka, *Adv. Sci.*, 2018, **5**, 1700526.

49 H. Fukunaga and H. Miyasaka, *Angew. Chem. Int. Ed.*, 2014, n/a-n/a.

50 E. Fernandez-Bartolome, P. Cruz, L. A. Galán, M. Cortijo, P. Delgado-Martínez, R. González-Prieto, J. L. Priego and R. Jiménez-Aparicio, *Polymers*, 2020, **12**, 1868.

51 W. Kosaka, Z. Liu, J. Zhang, Y. Sato, A. Hori, R. Matsuda, S. Kitagawa and H. Miyasaka, *Nat Commun*, 2018, **9**, 5420.

52 J. Zhang, W. Kosaka, Y. Kitagawa and H. Miyasaka, *Angew Chem Int Ed*, , DOI:10.1002/anie.202115976.

53 H. Ishida, M. Handa, I. Hiromitsu, S. Ujiie, D. Yoshioka, R. Mitsuhashi and M. Mikuriya, *New J. Chem.*, 2019, **43**, 1134–1145.

54 W. Kosaka, Y. Ishii and H. Miyasaka, *Polyhedron*, 2013, **52**, 1213–1218.

55 M. Itoh, Y. Asai, H. Kamo, A. Miura and H. Miyasaka, *Chem. Lett.*, 2012, **41**, 26–28.

56 D. J. Thompson, J. E. Barker Paredes, L. Villalobos, M. Ciclosi, R. J. Elsby, B. Liu, P. E. Fanwick and T. Ren, *Inorganica Chimica Acta*, 2015, **424**, 150–155.

57 N. Komiya, T. Nakae, H. Sato and T. Naota, *Chem. Commun.*, 2006, 4829.

58 S.-I. Murahashi, Y. Okano, H. Sato, T. Nakae and N. Komiya, *Synlett*, 2007, **2007**, 1675–1678.

59 W. Kosaka, Y. Watanabe, K. H. Aliyah and H. Miyasaka, *Dalton Trans.*, 2022, **51**, 85–94.

60 S. Furukawa and S. Kitagawa, *Inorg. Chem.*, 2004, **43**, 6464–6472.

61 M. C. Barral, R. González-Prieto, R. Jiménez-Aparicio, J. L. Priego, M. R. Torres and F. A. Urbanos, *Inorganica Chimica Acta*, 2005, **358**, 217–221.

62 H. Miyasaka, N. Motokawa, R. Atsuumi, H. Kamo, Y. Asai and M. Yamashita, *Dalton Trans.*, 2011, **40**, 673–682.

63 R. Gracia and N. J. Patmore, *J Clust Sci*, 2010, **21**, 339–350.

64 Y. Sekine, K. H. Aliyah, T. Shimada, J. Zhang, W. Kosaka and H. Miyasaka, *Chem. Lett.*, 2018, **47**, 693–696.

65 M. H. Chisholm, G. Christou, K. Folting, J. C. Huffman, C. A. James, J. A. Samuels, J. L. Wesemann and W. H. Woodruff, *Inorg. Chem.*, 1996, **35**, 3643–3658.

66 W. Kosaka, M. Itoh and H. Miyasaka, *Dalton Trans.*, 2015, **44**, 8156–8168.

67 S. Takamizawa, E. Nakata and T. Akatsuka, *Angew. Chem. Int. Ed.*, 2006, **45**, 2216–2221.

68 S. Takamizawa, E. Nakata, T. Akatsuka, C. Kachi-Terajima and R. Miyake, *J. Am. Chem. Soc.*, 2008, **130**, 17882–17892.

69 S. Takamizawa, E. Nakata and T. Saito, *Inorganic Chemistry Communications*, 2003, **6**, 1415–1418.

70 S. Takamizawa, E. Nakata, H. Yokoyama, K. Mochizuki and W. Mori, *Angew. Chem. Int. Ed.*, 2003, **42**, 4331–4334.

71 S. Takamizawa, E. Nataka, T. Akatsuka, R. Miyake, Y. Kakizaki, H. Takeuchi, G. Maruta and S. Takeda, *J. Am. Chem. Soc.*, 2010, **132**, 3783–3792.

72 S. Takamizawa, E. Nakata and T. Saito, *Inorganic Chemistry Communications*, 2004, **7**, 125–127.

73 W. Kosaka, K. Yamagishi, A. Hori, H. Sato, R. Matsuda, S. Kitagawa, M. Takata and H. Miyasaka, *J. Am. Chem. Soc.*, 2013, **135**, 18469–18480.

74 S. Takamizawa and R. Miyake, *CrystEngComm*, 2010, **12**, 2728.

75 W. Kosaka, K. Yamagishi, H. Yoshida, R. Matsuda, S. Kitagawa, M. Takata and H. Miyasaka, *Chem. Commun.*, 2013, **49**, 1594–1596.

76 T. Itoh, M. Kondo, M. Kanaike and S. Masaoka, *CrystEngComm*, 2013, **15**, 6122.

77 T. Itoh, M. Kondo, H. Sakamoto, K. Wakabayashi, M. Kanaike, K. Itami and S. Masaoka, *Dalton Trans.*, 2015, **44**, 15334–15342.

78 F. A. Cotton and J. L. Thompson, *Inorganica Chimica Acta*, 1984, **81**, 193–203.

79 D. P. Bancroft, F. A. Cotton and S. Han, *Inorg. Chem.*, 1984, **23**, 2408–2411.

80 F. A. Cotton, E. A. Hillard and C. A. Murillo, *J. Am. Chem. Soc.*, 2002, **124**, 5658–5660.

81 C. J. Simmons, A. Clearfield and Y. Sun, *Inorganica Chimica Acta*, 1986, **121**, L3–L6.

82 N. N. Sveshnikov, M. H. Dickman and M. T. Pope, *Acta Crystallogr C Cryst Struct Commun*, 2000, **56**, 1193–1195.

83 Y. Kim, S.-J. Kim and A. J. Lough, *Polyhedron*, 2001, **20**, 3073–3078.

84 T. Nozaki, W. Kosaka and H. Miyasaka, *CrystEngComm*, 2012, **14**, 5398.

85 Y. Kataoka, R. Fukumoto, N. Yano, D. Atarashi, H. Tanaka, T. Kawamoto and M. Handa, *Molecules*, 2019, **24**, 447.

86 S. Höfler, A. Scheja, B. Wolfram and M. Bröring, *Z. anorg. allg. Chem.*, 2016, **642**, 107–117.

87 T. Tsuchiya, R. Umemura, M. Kaminaga, S. Kushida, K. Ohkubo, S. Noro and Y. Mazaki, *ChemPlusChem*, 2019, **84**, 655–664.

88 D. K. Kumar, A. S. Filatov, M. Napier, J. Sun, E. V.

Dikarev and M. A. Petrukhina, *Inorg. Chem.*, 2012, **51**, 4855–4861.

89 V. Levchenko, B. Sundsli, S. Øien-Ødegaard, M. Tilset, F. K. Hansen and T. Bonge-Hansen, *Eur. J. Org. Chem.*, 2018, **2018**, 6150–6157.

90 H. J. Callot, A. M. Albrecht-Gary, M. Al Joubbeh, B. Metz and F. Metz, *Inorg. Chem.*, 1989, **28**, 3633–3640.

91 P. Chinapang, H. Iwami, T. Enomoto, T. Akai, M. Kondo and S. Masaoka, *Inorg. Chem.*, 2021, **60**, 12634–12643.

92 M. J. Bennett, W. K. Bratton, F. A. Cotton and W. R. Robinson, *Inorg. Chem.*, 1968, **7**, 1570–1575.

93 F. A. Cotton, T. Ren and M. J. Wagner, *Inorg. Chem.*, 1993, **32**, 965–968.

94 R. Gracia and N. J. Patmore, *Dalton Trans.*, 2013, **42**, 13118.

95 F. Neese, ORCA (version v. 4.2.1) 2018.

96 L. E. Roy, E. R. Batista and P. J. Hay, *Inorg. Chem.*, 2008, **47**, 9228–9237.

97 A. D. Becke, *Phys. Rev. A*, 1988, **38**, 3098–3100.

98 J. P. Perdew, *Phys. Rev. B*, 1986, **33**, 8822–8824.

99 F. Weigend and R. Ahlrichs, *Phys. Chem. Chem. Phys.*, 2005, **7**, 3297.

100 E. van Lenthe, E. J. Baerends and J. G. Snijders, *The Journal of Chemical Physics*, 1993, **99**, 4597–4610.

101 D. A. Pantazis, X.-Y. Chen, C. R. Landis and F. Neese, *J. Chem. Theory Comput.*, 2008, **4**, 908–919.

102 M. Bühl, C. Reimann, D. A. Pantazis, T. Bredow and F. Neese, *J. Chem. Theory Comput.*, 2008, **4**, 1449–1459.

103 D. M. York and M. Karplus, *J. Phys. Chem. A*, 1999, **103**, 11060–11079.

104 L. E. Roy, E. Jakubikova, M. G. Guthrie and E. R. Batista, *J. Phys. Chem. A*, 2009, **113**, 6745–6750.

105 L. P. Hammett, *J. Am. Chem. Soc.*, 1937, **59**, 96–103.

106 M. J. Bennett, K. G. Caulton and F. A. Cotton, *Inorg. Chem.*, 1969, **8**, 1.

107 F. A. Cotton, B. G. DeBoer, M. D. LaPrade, J. R. Pipal and D. A. Ucko, *Acta Crystallogr B Struct Crystallogr Cryst Chem*, 1971, **27**, 1664–1671.

108 A. Vega, V. Calvo, J. Manzur, E. Spodine and J.-Y. Saillard, *Inorg. Chem.*, 2002, **41**, 5382–5387.

109 M. A. Castro, Z. D. Chaia, O. E. Piro, F. D. Cukiernik, E. E. Castellano and M. Rusjan, *Acta Crystallogr C Cryst Struct Commun*, 2002, **58**, m393–m395.

110 F. A. Cotton, V. M. Miskowski and B. Zhong, *J. Am. Chem. Soc.*, 1989, **111**, 6177–6182.

111 F. A. Cotton, C. Lin and C. A. Murillo, *Inorg. Chem.*, 2000, **39**, 4574–4578.

112 F. Albert Cotton and R. Poli, *Polyhedron*, 1987, **6**, 1625–1628.

113 M. Huang, T. Yang, J. D. Paretsky, J. F. Berry and J. M. Schomaker, *J. Am. Chem. Soc.*, 2017, **139**, 17376–17386.

114 T. Ren, *Coordination Chemistry Reviews*, 1998, **175**, 43–58.

115 T. Ren, C. Lin, E. J. Valente and J. D. Zubkowski, *Inorganica Chimica Acta*, 2000, **297**, 283–290.

116 M. A. S. Aquino, *Coordination Chemistry Reviews*, 1998, **170**, 141–202.

117 S. M. Tetrick, V. T. Coombe, G. A. Heath, T. A. Stephenson and R. A. Walton, *Inorg. Chem.*, 1984, **23**, 4567–4570.

118 E. Van Caemelbecke, T. Phan, W. R. Osterloh and K. M. Kadish, *Coordination Chemistry Reviews*, 2021, **434**, 213706.

119 B. E. Bursten, F. A. Cotton, P. E. Fanwick, G. G. Stanley and R. A. Walton, *Chemischer Informationsdienst*, , DOI:10.1002/chin.198332053.

120 S. Mandal, S. Mallick, P. Garu, J. Chowdhury, A. Samadder, J. Das, A. R. Khuda-Bukhsh and S. Chattopadhyay, *New J. Chem.*, 2020, **44**, 4081–4091.

121 K. P. Kornecki, D. C. Powers, T. Ritter and J. F. Berry, *Progress in Inorganic Chemistry*, John Wiley & Sons, Hoboken, 2014, vol. 58.

122 T. Kawamura, M. Maeda, M. Miyamoto, H. Usami, K. Imaeda and M. Ebihara, *J. Am. Chem. Soc.*, 1998, **120**, 8136–8142.

123 A. Varela-Álvarez, T. Yang, H. Jennings, K. P. Kornecki, S. N. Macmillan, K. M. Lancaster, J. B. C. Mack, J. Du Bois, J. F. Berry and D. G. Musaev, *J. Am. Chem. Soc.*, 2016, **138**, 2327–2341.

124 O. Almog, A. Bino and D. Garfinkel-Shweky, *Inorganica Chimica Acta*, 1993, **213**, 99–102.

125 I. B. Baranovsky, M. A. Golubichnaya, P. A. Koz'min, M. D. Surazhskaya and N. K. Zh, *Russ. J. Inorg. Chem.*, 1995, 1634.